Electrical Excitation of Surface Plasmons by an Individual Carbon Nanotube Transistor

P. Rai,[1] N. Hartmann,[2] J. Berthelot,[1] J. Arocas,[1] G. Colas des Francs,[1] A. Hartschuh,[2] and A. Bouhelier[1,*]

[1]*Laboratoire Interdisciplinaire Carnot de Bourgogne, CNRS-UMR 6303, Université de Bourgogne, 21078 Dijon, France*

[2]*Department Chemie and CeNS, Ludwig-Maximilians-Universität, München 81377, Germany*

(Received 29 March 2013; published 11 July 2013)

We demonstrate here the realization of an integrated, electrically driven, source of surface plasmon polaritons. Light-emitting individual single-walled carbon nanotube field effect transistors were fabricated in a plasmonic-ready platform. The devices were operated at ambient conditions to act as an electroluminescence source localized near the contacting gold electrodes. We show that photon emission from the semiconducting channel can couple to propagating surface plasmons developing in the electrical terminals. Our results show that a common functional element can be operated for two different platforms emphasizing thus the high degree of compatibility between state-of-the-art nano-optoelectronics devices and a plasmonic architecture.

DOI: 10.1103/PhysRevLett.111.026804 PACS numbers: 73.20.Mf, 73.63.Fg, 85.35.Kt

Plasmonics is emerging as an alternative technology to satisfy constrains of miniaturization of optical devices down to subwavelength sizes [1–3]. This on-chip technology utilizes the unique properties of surface plasmon polariton (SPP) to transmit optical and electrical signals through the same metal-based circuitry. A complete plasmonic platform requires the development of elementary building blocks with specific functionalities including routing and modulating SPPs, but also on-chip excitation and detection [2,4,5]. The vast majority of fabricated plasmonic prototypes rely on an optical excitation of SPPs, typically involving laser sources and macroscopic coupling elements [6,7]. Despite optimized SPP coupling efficiencies, these external sources can hardly be integrated on the nanoscale, and novel routes for in-out connections are needed. An electrical excitation and detection of SPPs offers dramatic advantages over standard coupling schemes. Electrical terminals can be readily integrated offering thus a hybrid technology to interface miniature electronic devices with a plasmonic architecture [8–12].

In this context, the unique opto-electronic properties of carbon nanotubes [13–15] could provide a novel approach for integrating SPP nanosources in complex interconnected systems. Single-walled carbon nanotubes (SWNTs) feature well-defined electronic resonances in the visible to near-infrared spectral range and can sustain extremely high current densities [14,16]. Bright, stable, and localized infrared emission was observed from individual SWNT field effect transistors (SWNTFETs) demonstrating their usability as nanoscale light emitting devices [14,15]. SWNTs could thus offer a new integration route enabling a local plasmon excitation in an electrical circuitry combining a transistor and a SPP generator in a single unit superseding complex fabrication procedures.

In this article we demonstrate coupling of the radiation emitted by an individual electrically driven SWNTFET to SPPs developing in waveguidelike electrodes. Electroluminescence (EL) from the device is obtained by an impact excitation process under unipolar transport of carriers in the semiconducting channel. Our SPP excitation scheme employs the same gate-controlled functional element widely used as the elementary unit in nanoelectronics providing thus a high degree of integration with existing technologies.

SWNTFETs were fabricated by electron beam lithography and lift off processes on a glass cover slip. Device schematics are shown in Fig. S1 of the Supplemental Material [17]. Electrical gating was ensured by evaporating a 30 nm thick conductive layer of transparent indium tin oxide (ITO). A 250 nm thick layer of SiO_2 was then deposited onto the ITO to act as a dielectric spacer. High-pressure carbon monoxide synthesized SWNTs [18,19] were randomly deposited from a solution on the prepared ITO-gated substrate. Nanotubes were located by scanning electron microscopy (SEM) before lithography of the electrical source and drain contacts. The leads were formed by depositing 5 to 10 nm of Pd or Ti followed by 45 nm of Au. Pd or Ti were employed to reduce the Schottky barrier for majority carriers in the nanotube [13,14] while Au was used for its compatibility to simultaneously transport electrons and SPPs. The inset of Fig. 1(a) shows a SEM image of a $\sim 0.8\ \mu$m long SWNTFET. The contrast was saturated to distinguish the nanotube from the electrodes. Drain was maintained at ground potential. The diameter of the nanotube is ~ 0.75 nm as measured with atomic force microscopy (data not shown). The output characteristics (I_{DS}-V_{DS}) of the device for several gate bias (V_{GS}) are presented in Fig. 1(a). The drain current (I_{DS}) is increasing with negative gate bias. Figure 1(b) displays the electrical transfer characteristics (I_{DS}-V_{GS}) for different V_{DS} showing a p-channel metal-oxide-semiconductor field-effect transistor behavior. The ON/OFF ratio of the transistor is here ~ 50. All the devices fabricated on glass cover slips

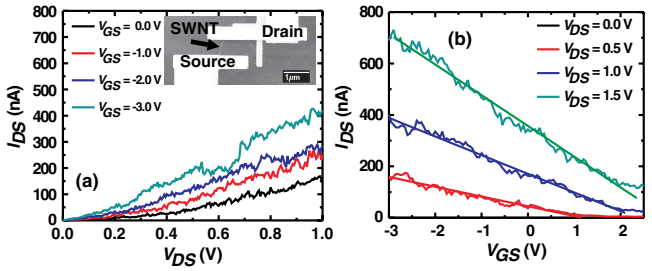

FIG. 1 (color online). (a) The electrical output and (b) transfer characteristics of a SWNTFET. A straight line fitting follows the transport equation of the device. The inset in (a) shows a SEM image of the SWNTFET fabricated on a glass cover slip.

behaving like FETs showed that the majority of carriers were dominated by holes. The origin of the p-type conduction in our device is mainly due to the Schottky barrier formation at the nanotube-metal contacts [13,14] and its operation at ambient conditions [20]. A large variation of the ON/OFF ratio from device to device was observed ranging from 10^4 down to a few units.

EL in a SWNTFET such as the one displayed in Fig. 1(a) can be achieved through different mechanisms: impact excitation [14], recombination of carriers during ambipolar transport [15], phonon-assisted process [21], and recombination from thermally populated electronic states [22,23]. Figure 2(a) shows the EL emission of a typical SWNTFET fabricated on a glass substrate. The image is overlaid with an image of the electrode geometry obtained under a weak wide-field illumination recorded with an inverted optical microscope equipped with a 100 ×, 1.49 numerical aperture (N.A.) objective and an imaging spectrometer. The EL

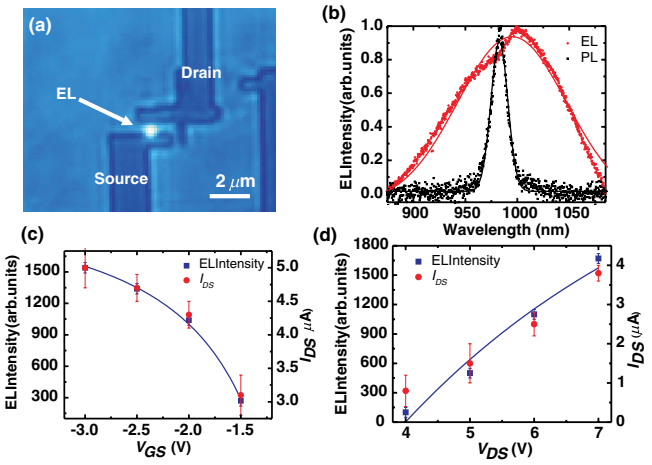

FIG. 2 (color online). (a) EL activity of the SWNTFET at $V_{GS} = -3$ V, $V_{DS} = 6$ V and for an integration time of 60 s. (b) Normalized PL and EL spectrum. (c) Plot of EL intensity (blue squares) and drain current (red circles) versus gate bias at constant $V_{DS} = 6$ V. (d) Plot of EL intensity and drain current versus drain bias at constant $V_{GS} = -2$ V. The solid blue lines in (c) and (d) are fits of Eq. (1) to the experimental data.

image was recorded at $V_{DS} = 6$ V and $V_{GS} = -3$ V for 60 s. Within the resolution of the microscope (~ 500 nm corresponding to two pixels of the camera), EL emission is observed over the entire length of the channel. To identify the optical transition responsible for EL emission, we compared the EL spectrum to the photoluminescence (PL) spectrum of an individual nanotube from the same colloidal solution placed on the same substrate. This procedure was necessary because the nanotubes did not show PL emission after imaging by SEM during the device fabrication [19]. The EL (red circles) and PL (black squares) spectra are shown together in Fig. 2(b), and peak at 995 and 982 nm, respectively. The solid lines are Gaussian fits to the corresponding spectra. The emission correlates with the E_{11} transition of (6,5) nanotubes. The EL spectrum is broadened compared to the PL spectrum probably due to the involvement of various vibrational states excited during electronic transport [22]. The width of the EL band of about 110 nm is slightly larger than what has been observed for other single SWNT devices [24]. This is expected since non radiative coupling in the metal contacts reduces the exciton lifetime substantially. A small redshift in the EL may be caused by drain-induced doping [25] and the shoulder in the EL band could indicate emission from nominally dark states that can be observed for defective nanotubes and nanotubes on substrates [24,26].

We hypothesize that an impact excitation process is responsible for EL emission because the emission intensity depends on the application of a bias voltage. In short channel SWNTFETs, the combined electric fields applied between source and drain and between source and gate produce a sufficiently high electric field at the metal-nanotube interface to accelerate the carriers (~ MV/cm estimated from the voltage applied to the channel). Thus, holes injected into the valence band are accelerated towards the drain by the large potential difference. The accelerated holes may produce singlet excitons by impact excitation, which can decay radiatively [14]. Impact excitation-driven EL in integrated plasmonic devices is an important mechanism compared to other EL processes. For thermal emission and phonon-assisted EL, the emission is located at the center of a quasimetallic channel [21,23]. The surface plasmon receptacle, i.e., the electrodes, are therefore distant from the EL source. SPP excitation requires the near-field proximity of the electroluminescent source; coupling to a plasmon is hence unlikely for these two EL processes. Under proper gating conditions, charge recombination under ambipolar transport may occur at the electrodes. Coupling to an SPP should thus be possible. However, compared to impact excitation, the radiative yield under ambipolar transport was reported to be two to three orders of magnitude lower [14]. For an efficient plasmon launching, impact excitation is hence the favored mechanism as it provides brighter EL localized at the electrode interface. Impact excitation

requires conserving both energy and momentum. Momentum conservation increases the threshold energy by a factor of 1.5 with respect to the minimum energy necessary for exciton formation [27].

The threshold electric field (F_{th}) for impact excitation is given by $\sim 1.5E_g/e\lambda_{\mathrm{ph}}$, where E_g and λ_{ph} are the optical band gap and optical phonon scattering length of the SWNT, respectively. E_g deduced from the EL/PL emission is about 1.25 eV. λ_{ph} is approximately 15–20 nm for SWNTs [28]. F_{th} is thus estimated to be 0.9–1.2 MV/cm. The EL emission intensity depends on the impact excitation rate with an exponent equal to $[-F_{\mathrm{th}}/F_{\mathrm{app}}]$, where F_{app} is the effective electric field applied to the metal-nanotube interface [27]. This electric field can be expressed as $F_{\mathrm{app}} = [\gamma V_{DS} + (V_{GS} - V_T)]/\lambda_{\mathrm{scr}}$, where γ is the fraction of V_{DS} contributing to the impact excitation rate, λ_{scr} is the screening length that represents the length over which the potential drops within the metal-nanotube junction [29] and V_T is the turn-on voltage for the device. Thus, the EL emission intensity (S_{el}) is given by the expression

$$S_{\mathrm{el}} \sim \exp[-F_{\mathrm{th}}\lambda_{\mathrm{scr}}/(\gamma V_{DS} + (V_{GS} - V_T))]. \quad (1)$$

The screening length for impact excitation in SWNTFET devices is $\lambda_{\mathrm{scr}} = \sqrt{\varepsilon_{\mathrm{cnt}} d_{\mathrm{cnt}} t_{\mathrm{ox}}/\varepsilon_{\mathrm{ox}}}$ [29], where $\varepsilon_{\mathrm{cnt}}$ and d_{cnt} are the dielectric constant and diameter of the SWNT, respectively, and $\varepsilon_{\mathrm{ox}}$ and t_{ox} are the dielectric constant and thickness of the oxide layer, respectively. The screening length is estimated to be $\sim$19 nm by using $\varepsilon_{\mathrm{cnt}} = 7.5$ [30], $d_{\mathrm{cnt}} = 0.75$ nm, $\varepsilon_{\mathrm{ox}} = 4$ and $t_{\mathrm{ox}} = 250$ nm. The transport of SWNTFET is governed by the equation, $I_{DS} = \mu C/L^2 V_{DS}(V_{GS} - V_T)$, where μ is the carrier mobility, C is the geometrical capacitance and L is the channel length [31]. The geometrical capacitance is $C = 2\pi\varepsilon_{\mathrm{ox}}/\ln(2t_{\mathrm{ox}}/d_{\mathrm{cnt}}) = 0.04$ aF/nm [32]. $V_T \sim 2.2$ V and mobility $\mu \sim 25\ \mathrm{cm}^2\,\mathrm{V/s}$ for holes are deduced by a straight line fitting of the transfer characteristics with the transport equation [Fig. 1(b)].

To confirm that impact excitation is responsible for light emission in our devices, we recorded the emission intensity by varying the bias voltages. Figure 2(c) shows the plot of I_{DS} and EL emission intensity versus gate bias, keeping V_{DS} constant at 6 V. The EL intensity was obtained by integrating the photon counts received by the camera in an area corresponding to the length of the channel. Both EL intensity (blue squares) and I_{DS} (red circles) are showing the same dependence on the gate bias demonstrating the relationship between the number of carriers in the channel and the EL activity. The evolution with V_{GS} is well reproduced by Eq. (1) as shown by the solid blue line in Fig. 2(c) with $\gamma = 0.36$. The remaining V_{DS} may be attributed to carrier transport and thermal heating in the nanotube. Figure 2(d) depicts the EL response with drain bias for $V_{GS} = -2$ V (blue squares). The current injected in the channel is shown with red circles. Here too, there is an obvious correspondence between the EL activity and the drain-controlled current running through the transistor. The trend is well described by Eq. (1) (blue curve) with the same value of γ as in Fig. 2(c). Unlike the mobile EL emission under ambipolar transport conditions [15], the stationary nature of the EL site and its gate-dependent intensity strongly suggest that impact excitation is responsible for light emission. In contrast, phonon-assisted relaxation would lead to two weak emission bands centered at around 950 and 700 nm [21] and can therefore be excluded based on the observed EL spectrum.

We fabricated longer channel SWNTFET with specifically designed electrode geometries [Fig. 3(a)] to demonstrate that the EL emission of the channel can be coupled to propagating SPPs in the electrical terminals. The device was driven at $\sim 1\ \mu$A drain current continuously for 30 s to acquire EL emission images displayed in Figs. 3(b)–3(d) for different V_{GS}. EL from the device is observed at both the source-nanotube and the drain-nanotube contacts for $V_{DS} = 16$ V and $V_{GS} = -9$ V [Fig. 3(b)]. The emission intensity at the source-nanotube contact increases with gate bias. Interestingly, we observe light emitted from the edge of the source electrode separated from the nanotube by about 2 μm at V_{GS} of -10 V [Fig. 3(c)]. The intensity of light at the extremity is related to the intensity of the electroluminescent activity at the nanotube contact with a ratio of 0.32 in both Figs. 3(c) and 3(d). Light emitted at the end facet of the electrode is a strong indication supporting the excitation of surface plasmons propagating in the source terminal. SPPs are thus developing in an electrode that also serves as a metal waveguide [33]. At the extremity, SPPs are scattered and are partially converted to detectable photons [9,10,34]. We found that a thickness <5 nm of the Pd or Ti adhesion layer was necessary to observe SPPs. We were not able to confirm its excitation for thicker layers, probably due to an increase SPP damping.

Coupling to SPPs requires a resonant in-plane wave vector and a component of the field polarized along the propagation direction. EL emission in SWNTs is known to be polarized along the axis of the nanotube [35] as shown

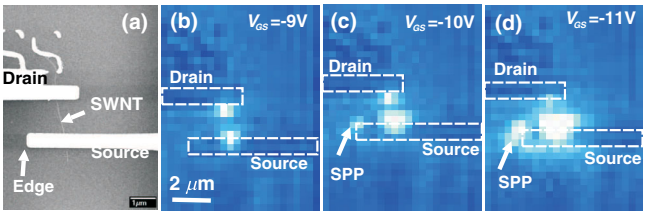

FIG. 3 (color online). (a) SEM image of a $\sim 1.8\ \mu$m-long SWNTFET. (b), (c), and (d) are overlaid EL images with $V_{GS} = -9, -10, -11$ V, respectively, at $V_{DS} = 16$ V. Scattering of light from the edge of the source electrode as shown in (c) and (d) demonstrates the excitation of SPP by the EL of the device.

in Fig. S2 [17]. In the device displayed in Fig. 3(a), the nanotube is oriented at 75° with respect to the source electrode. Thus, there is a small component of the electric field oriented along the main axis of the source electrode that can couple to SPPs. The SPP to EL intensity ratio versus nanotube orientation (Fig. S3 of the Supplemental Material [17]) shows a weaker coupling for SWNTs tilted from the electrode interface. Furthermore, the mechanism responsible for EL has a limited spatial extension. According to Fig. 3, the size of the source is shorter than the wavelength-scale dimension of the channel. This confinement near the metal-nanotube interface indicates that the near-field source possesses a broad distribution of momentum, some of them resonant with SPPs.

To realize an electrical excitation of SPPs in a bias-free electrode, we fabricated a SWNTFET by placing an additional receiving SPP waveguide on top of the nanotube channel. Figure 4(a) shows the EL activity from such a device at $V_{DS} = 10$ V and $V_{GS} = -5$ V. Strong responses at the contacts are observed again concomitant to weaker signals appearing at the left edges of the metal leads and of the bias-free waveguide. This scattered light emitted from the metal further confirms that SPPs can be excited with an electroluminescent plasmonic-compatible SWNTFET.

To determine the nature of the excited SPP mode, we theoretically calculated the effective index of the mode and its propagation length for our device geometry and emission wavelength. The dielectric constants for SiO_2, Ti, Au, and air at 980 nm wavelength are $\varepsilon_{SiO_2} = 2.25$, $\varepsilon_{Ti} = 0.3 + i21.5$, $\varepsilon_{Au} = -39.9 + i2.7$, and $\varepsilon_{air} = 1$, respectively. The effective index and propagation length for a SPP mode at the Au/air interface are calculated to be 1.01 and 40 μm, respectively. For the Au thickness considered here, this SPP mode would loose part of its energy in the substrate and should be detected as leakage radiation [34]. There is, however, no evidence of the presence of this leaky mode in the EL images presented in Figs. 3 and 4.

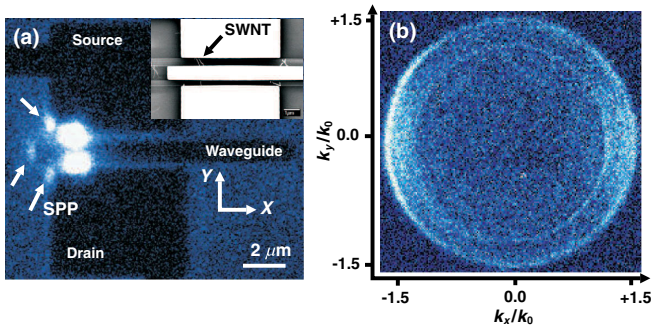

FIG. 4 (color online). (a) EL-coupled SPPs launched in the source, drain, and waveguide electrodes for $V_{GS} = -5$ V and $V_{DS} = 10$ V and an integration time of 120 s. Inset: SEM image of a SWNTFET integrated with a plasmonic compatible waveguide placed on top of the nanotube channel. (b) Fourier space image of the corresponding EL-coupled SPP shown in (a).

Propagation of a leaky SPP mode is conditioned by the waveguide dimensions. A cutoff condition exists that is approximately equal to the free space wavelength of the light emitted [33,34,36]. In our configuration the width of the electrodes are below cutoff and the leaky mode is therefore vanishing. The second relevant SPP mode is a bound mode developing at the glass-metal interface. Its effective index and propagation length are 1.56 and 3 μm, respectively. We hypothesize that the SPP excited in the device configuration presented here is indeed the bound mode. To confirm this assumption, we display in Fig. 4(b) the momentum-space distribution of the EL emission [18,34]. The detection is limited by the objective N.A. at 1.49. The critical angle at the glass-air interface is readily recognized ($k/k_0 = 1.0$). There is no indication of a leaky propagating SPP mode in this wave-vector distribution [34]. Instead, most of the light is emitted in a two-lobe pattern symmetric with respect to the reciprocal k_x/k_0 axis. Since the EL intensity at the contacts are the predominant signals in Fig. 4(b), the momentum distribution essentially reflects the dipolarlike emission pattern of the nanotube [18]. A maximum of intensity is observed at the outer rim for negative values of k_x/k_0. These observations are consistent with our original assumption: SPPs propagating along the waveguides are scattered out at the left extremities. Since these edges are located at 1.5 to 2 μm from the channel, a distance smaller than the propagation length of the bound SPP mode, a substantial fraction of the SPP amplitude is able to reach the edge. Scattering of the SPPs by the sharp terminations is occurring at large wave vectors explaining the rise of intensity near the angular detection limit at -1.49. SPPs are probably excited in both directions but, because the right extremities of the electrodes are located more than 6 μm away from the EL site, the SPPs decay before reaching the edges and remain undetected.

In summary, we have demonstrated the use of a SWNT-based opto-electronic device to produce an integrated electrical source of SPPs. Light emission in the device is generated by a radiative relaxation of excitons formed by impact excitation. EL is partly coupled to bound SPPs that are conjointly transported with the electrical command in the SWNTFET plasmonic-compatible terminals. In our devices, the coupling yield was limited by the relative orientation of the nanotube with respect to the electrode geometry, a limitation that can be addressed by an adapted device design. Additional SPP routing and filtering functions could also be easily implemented by fine structuring the electrodes. Finally, the transfer characteristics of SWNTFETs can be electrically modulated up to the MHz regime. Since the electroluminescent response and the SPP signal directly depend on the biasing condition, the device presented here could also serve to electrically modulate the surface plasmon intensity, a prerequisite to encode optical information in such a platform.

This work was funded partially by the NanoSci E+ program under Grant E^2-PLAS (ANR-08-NSCI-007), the regional council of Burgundy with the program PARI, the DFG through HA4405/5-1, and the Nanosystems Initiative Munich (NIM). This project has been performed in cooperation with the Labex ACTION program (Contract No. ANR-11-LABX-01-01).

*Corresponding author.
alexandre.bouhelier@u-bourgogne.fr

[1] W. L. Barnes, A. Dereux, and T. W. Ebbesen, Nature (London) **424**, 824 (2003).
[2] R. Zia, J. A. Schuller, A. Chandran, and M. L. Brongersma, Mater. Today **9**, 20 (2006).
[3] E. Ozbay, Science **311**, 189 (2006).
[4] T. W. Ebbesen, C. Genet, and S. I. Bozhevolnyi, Phys. Today **61**, No. 5, 44 (2008).
[5] M. Dragoman and D. Dragoman, Prog. Quantum Electron. **32**, 1 (2008).
[6] A. Bouhelier and G. P. Wiederrecht, Opt. Lett. **30**, 884 (2005).
[7] A. Hohenau, J. R. Krenn, A. L. Stepanov, A. Drezet, H. Ditlbacher, B. Steinberger, A. Leitner, and F. R. Aussenegg, Opt. Lett. **30**, 893 (2005).
[8] R. J. Walters, R. V. A. van Loon, I. Brunets, J. Schmitz, and A. Polman, Nat. Mater. **9**, 21 (2010).
[9] P. Neutens, L. Lagae, G. Borghs, and P. Van Dorpe, Nano Lett. **10**, 1429 (2010).
[10] P. Fan, C. Colombo, K. C. Y. Huang, P. Krogstrup, J. Nygard, A. Fontcuberta i Morral, and M. L. Brongersma, Nano Lett. **12**, 4943 (2012).
[11] P. Bharadwaj, A. Bouhelier, and L. Novotny, Phys. Rev. Lett. **106**, 226802 (2011).
[12] D. M. Koller, A. Hohenau, H. Ditlbacher, N. Galler, F. Reil, F. R. Aussenegg, A. Leitner, E. List, and J. Krenn, Nat. Photonics **2**, 684 (2008).
[13] P. Avouris, M. Freitag, and V. Perebeinos, Nat. Photonics **2**, 341 (2008).
[14] J. Chen, V. Perebeinos, M. Freitag, J. Tsang, Q. Fu, J. Liu, and P. Avouris, Science **310**, 1171 (2005).
[15] M. Freitag, J. Chen, J. Tersoff, J. C. Tsang, Q. Fu, J. Liu, and P. Avouris, Phys. Rev. Lett. **93**, 076803 (2004).
[16] A. M. Rao *et al.*, Science **275**, 187 (1997).
[17] See Supplemental Material at http://link.aps.org/supplemental/10.1103/PhysRevLett.111.026804 for the additional figures and associated descriptions.
[18] N. Hartmann, G. Piredda, J. Berthelot, G. Colas des Francs, A. Bouhelier, and A. Hartschuh, Nano Lett. **12**, 177 (2012).
[19] P. Rai, N. Hartmann, J. Berthelot, G. C. des Francs, A. Hartschuh, and A. Bouhelier, Opt. Lett. **37**, 4711 (2012).
[20] G. U. Sumanasekera, C. K. W. Adu, S. Fang, and P. C. Eklund, Phys. Rev. Lett. **85**, 1096 (2000).
[21] S. Essig *et al.*, Nano Lett. **10**, 1589 (2010).
[22] M. Freitag, V. Perebeinos, J. Chen, A. Stein, J. C. Tsang, J. A. Misewich, R. Martel, and P. Avouris, Nano Lett. **4**, 1063 (2004).
[23] D. Mann, Y. K. Kato, A. Kinkhabwala, E. Pop, J. Cao, X. Wang, L. Zhang, Q. Wang, J. Guo, and H. Dai, Nat. Nanotechnol. **2**, 33 (2007).
[24] M. H. P. Pfeiffer, N. Stürzl, C. W. Marquardt, M. Engel, S. Dehm, F. Hennrich, M. M. Kappes, U. Lemmer, and R. Krupke, Opt. Express **19**, A1184 (2011).
[25] M. Freitag, M. Steiner, A. Naumov, J. P. Small, A. A. Bol, V. Perebeinos, and P. Avouris, ACS Nano **3**, 3744 (2009).
[26] A. Vijayaraghavan *et al.*, ACS Nano **4**, 2748 (2010).
[27] Y. Okuto and C. R. Crowell, Phys. Rev. B **6**, 3076 (1972).
[28] A. Javey, J. Guo, M. Paulsson, Q. Wang, D. Mann, M. Lundstrom, and H. Dai, Phys. Rev. Lett. **92**, 106804 (2004).
[29] A. D. Franklin, R. A. Sayer, T. D. Sands, T. S. Fisher, and D. B. Janes, J. Vac. Sci. Technol. B **27**, 821 (2009).
[30] J. A. Fagan *et al.*, Phys. Rev. Lett. **98**, 147402 (2007).
[31] R. Martel, T. Schmidt, H. R. Shea, T. Hertel, and P. Avouris, Appl. Phys. Lett. **73**, 2447 (1998).
[32] M. P. Anantram and F. Léonard, Rep. Prog. Phys. **69**, 507 (2006).
[33] J.-C. Weeber, J. R. Krenn, A. Dereux, B. Lamprecht, Y. Lacroute, and J. P. Goudonnet, Phys. Rev. B **64**, 045411 (2001).
[34] J. Berthelot, F. Tantussi, P. Rai, G. C. des Francs, J.-C. Weeber, A. Dereux, F. Fuso, M. Allegrini, and A. Bouhelier, J. Opt. Soc. Am. B **29**, 226 (2012).
[35] J. A. Misewich, R. Martel, P. Avouris, J. C. Tsang, S. Heinze, and J. Tersoff, Science **300**, 783 (2003).
[36] R. Zia, J. A. Schuller, and M. L. Brongersma, Phys. Rev. B **74**, 165415 (2006).